Journal of Marine Research, 43, 67–81, 1985

Evolution of sea-surface temperature in the tropical Atlantic Ocean during FGGE, 1979: II. Oceanographic fields and heat balance of the mixed layer

by Robert L. Molinari,[1] John F. Festa[1] and Eric Marmolejo[1]

ABSTRACT

Surface meteorological and surface and subsurface oceanographic data collected during 1979 are used to describe sea-surface temperature, mixed layer depth, zonal current component and net oceanic heat gain fields and to estimate the terms in a heat balance relation for the mixed layer. The terms are evaluated monthly on a 6° of latitude by 10° of longitude grid which covers the equatorial Atlantic from 9S to 9N. The first balance tested is between changes in mixed layer temperature and surface energy fluxes. These fluxes can account for more than 75% of the variance in the original time series of the quadrangles along 6S. Variance reductions are less along 0° (order of 50%) and 6N (less than 25%). The addition of zonal advection improves some of the predictions but not significantly. Low variance reductions along 6N, west of 20W are attributed to the uncertainties in the estimates of observed temperature change and surface fluxes. The small variance reductions east of 20W, at 6N and along 0° may be related to the neglect of coastal and equatorial upwelling and meridional advection. A simple model is proposed which assumes an annual cycle for the intensity of mixing across the base of the mixed layer, most intense during summer, least intense during winter. Variance reductions at 0°, 5W increase from 20% to 60% with the inclusion of mixing. Meridional advection may also account for a portion of the observed variability in mixed layer temperature.

1. Introduction

The equatorial Atlantic Ocean may play a large role in moderating global atmospheric climate, as heat gained through the sea-surface in this region may be transported poleward to compensate for radiation deficits at higher latitudes (Hastenrath, 1980). Sea-surface temperature (SST) is one of many variables which determines the magnitude of oceanic heat gain. The role of equatorial heat gain and SST in climate will ultimately be determined from the results of general circulation models (GCM's) of the coupled ocean-atmosphere system. The complexity of the GCM's will depend, in part, on the dynamics of SST variability. In the simplest case the ocean is passive (i.e., it stores heat locally in the summer and releases heat locally in the winter) and ocean dynamics do not play a role in SST variability. In the most complicated case

1. National Oceanic and Atmospheric Administration, Atlantic Oceanographic and Meteorological Laboratory, 4301 Rickenbacker Causeway, Miami, Florida, 33149, U.S.A.

the ocean is active (i.e., horizontal advection, upwelling, diffusion, etc. affect SST) and ocean dynamics must be included in the GCM's. Empirical studies of the evolution of SST will provide some initial guidance on which processes must be considered. In addition, the data and results from these studies can serve as constraints on the GCM results. Thus, we attempt to determine the dynamics of SST variability in the tropical Atlantic Ocean.

Previous studies using climatological data sets (Merle, 1980, for instance) have shown that internal oceanic processes do indeed affect SST variability. Molinari *et al.* (1983), using a combination of climatological data and data collected during the First GARP Global Experiment (FGGE) and a box-model developed by Wyrtki (1981), identified equatorial upwelling, zonal advection and vertical mixing as oceanic processes affecting equatorial Atlantic SST's. Herein, we utilize a development given by McPhaden (1982) and only data collected during FGGE to study the annual cycle of the equatorial Atlantic SST distribution. By using data from the same year, we hope to avoid many of the problems inherent in using climatological data sets such as the possible loss due to smoothing of phase relations between variables.

We explicitly evaluate the effects of sea-surface energy fluxes and zonal advection on the SST field and infer the effects of other processes such as entrainment and meridional advection. The region considered extends basin-wide from 9S to 9N and is divided into 6° of latitude by 10° of longitude quadrangles. The annual cycle is evaluated through analysis of mean monthly variables. Mean monthly fields of SST, mixed layer depth, surface current and net oceanic heat gain distributions were generated to perform this analysis. A brief description of these fields is also included.

2. Mixed layer heat balance

Following McPhaden (1982), we can express the heat balance of the mixed layer on monthly time scales as (we assume that mixed layer temperature is equivalent to SST):

$$\underset{1}{\frac{\partial T}{\partial t}} - \underset{2}{\frac{1}{\delta t}\left[T(t_1) - T(t_0)\right]} + \underset{3}{\left(u\frac{\partial T}{\partial x}\right)'} + \left(v\frac{\partial T}{\partial y}\right)' = \underset{4}{\frac{1}{\rho c_p}\left[\left(\frac{Q_o}{h}\right)'\right]} - \underset{5}{\left[\left(\frac{Q_{-h}}{h}\right)'\right]} \qquad (1)$$

where primes denote fluctuations about the mean. T is SST, t is time, $t_1 - t_0$ is record length, u is zonal current speed, h is mixed layer depth, Q_o is oceanic heat gain through the sea-surface and Q_{-h} is vertical turbulent heat diffusion. Thus, the change in mixed layer temperature, term 1 in Eq. (1), is expressed in terms of several mechanisms. Term 2 represents a correction for any trends in SST. This term is required since the mean value of the various mechanisms represented in (1) are subtracted from the monthly values. These means can cause trends in SST, trends caused by low-frequency fluctuations not adequately resolved by the one-year time series. Term 3 represents the

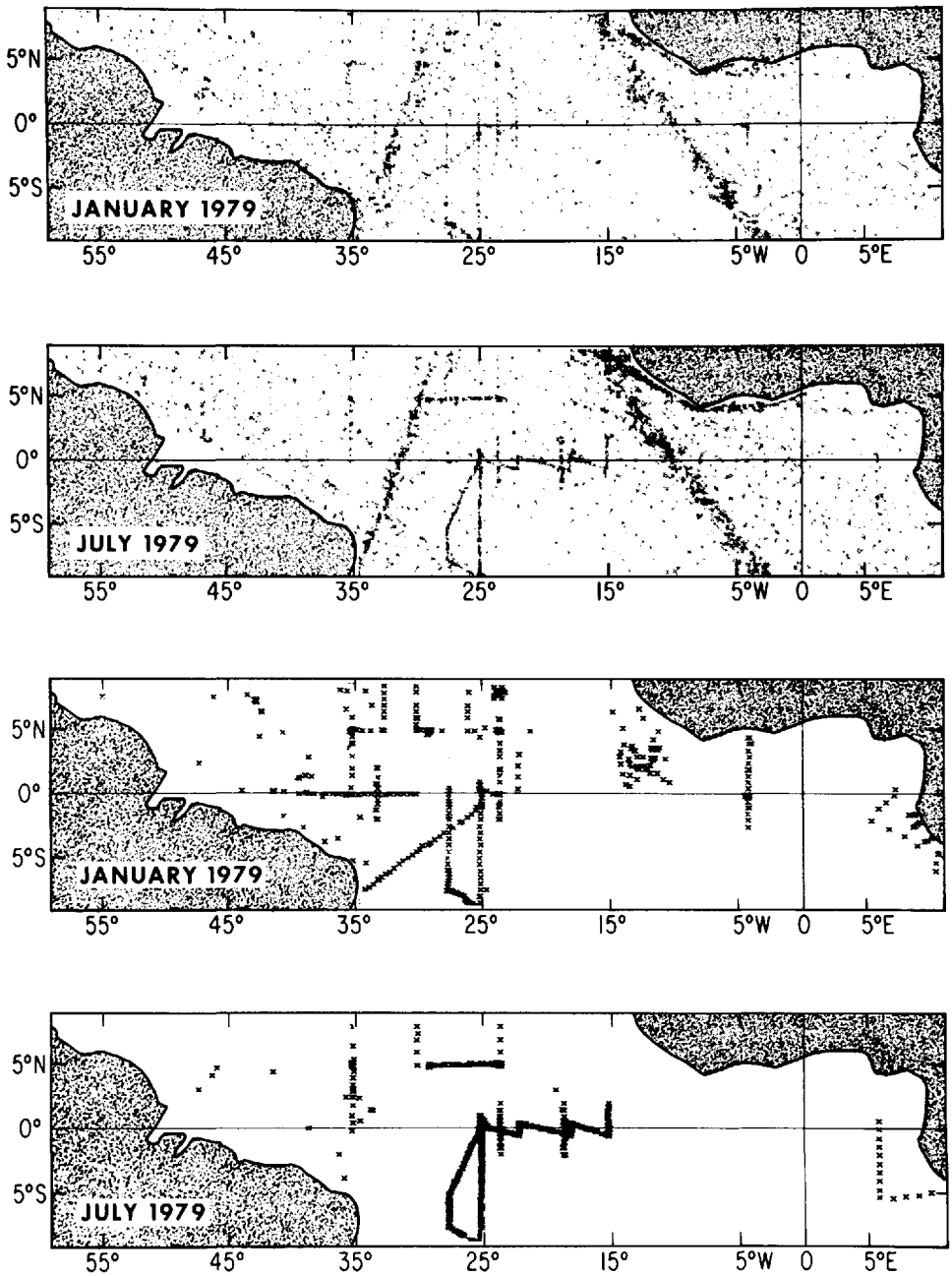

Figure 1. Distribution of surface (upper panel) and subsurface observations (lower panel) during February and August 1979.

effect of anomalies in zonal and meridional advection. Term 4 represents the effect of anomalies in net oceanic heat gain at the sea-surface. This heat gain is given by the sum of the net short and long-wave radiation balances and latent and sensible heat fluxes. Finally, term 5 represents anomalies of vertical turbulent diffusion through the base of the mixed layer. We ignore effects due to horizontal turbulent diffusion and attenuation of penetrative radiation.

3. Data sources

Molinari *et al.* (1984), hereinafter referred to as MFM, used data collected during FGGE to evaluate surface energy fluxes in the tropical Atlantic Ocean. In summary, ship-of-opportunity oceanographic and surface meteorological data (see Fig. 1 for some representative data distributions) were used in the bulk-exchange formulas to compute, on a 2° × 2° grid, monthly distributions of latent and sensible heat fluxes and net short and long-wave radiation balances. Net oceanic heat gain at each grid point is then given as the difference between incoming and outgoing fluxes. Errors in estimates of monthly heat gain due to uncertainties in the observations and inadequacies in the sampling (but independent of any shortcomings in the bulk formulation) are functions of grid position relative to the shipping lanes (Fig. 1). Within the shipping lanes, estimated errors are of the order of 45 W/m^2, outside the lanes errors are larger. However, as will be shown, actual errors are probably considerably less.

Subsurface oceanographic data are available from the extensive research vessel fleet deployed during FGGE (Fig. 1). Temperature profiles were obtained from XBT, CTD and Nansen stations and are used to determine mixed layer depth. The mixed layer depth is defined as the first depth at which the temperature is 0.5° less than the SST. Mixed layer depths can be determined from XBT and CTD data to within several meters. Maximum errors in mixed layer depths derived from Nansen casts are a function of bottle spacing, typically less than 25 m in the upper layers.

The distribution of subsurface data was uneven in both time and space (Fig. 1). Considerable smoothing and interpolation were required to obtain monthly values of mixed layer depth at all the grid points of the 6° of latitude by 10° of longitude grid. The mixed layer climatology of Lamb (1984) was used to perform the smoothing and interpolation. The procedure involved plotting the raw and climatological mixed layer depth values (Fig. 2). In regions of considerable data, e.g., in the bands 3S to 3N and 3N to 9N (Fig. 2), the raw values were generally used. In regions of fewer data, e.g., the 9S and 3S band (Fig. 2), the Lamb (1984) values were used to obtain a smooth time series. On the average, the estimates of mixed layer depth are probably accurate to ±10 m.

Surface current data are available in the form of ship drift reports obtained during FGGE and supplied by the British Meteorological Office and direct current observations from research vessels. The former representations of surface current can be contaminated by wind effects on ship drift. The error is likely to be systematic rather

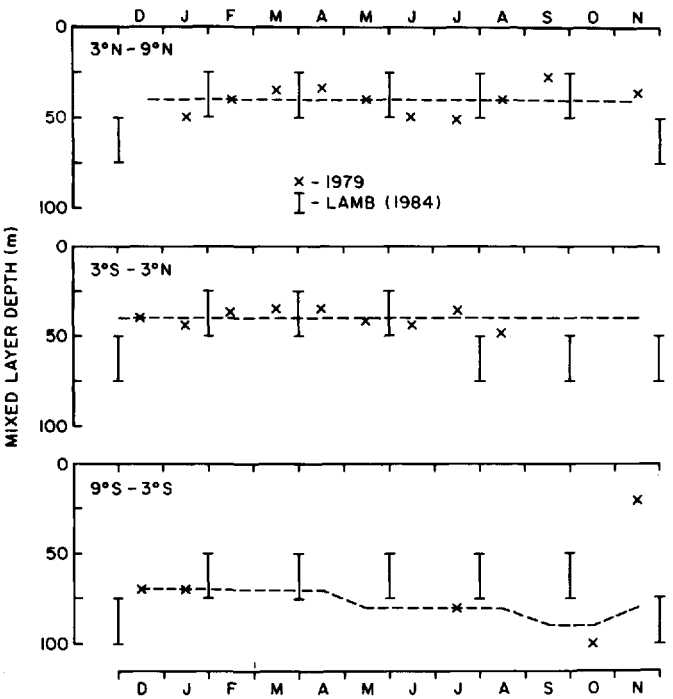

Figure 2. Observed, climatological (Lamb, 1984) and interpolated mixed layer depths (m) for the three quadrangles along 25W. The numbers represent the observations available during 1979. The length of the bars is equivalent to the contour interval (25 m) used by Lamb (1984).

than random, as the dominant winds in the eastern Atlantic are southerly and in the western Atlantic, easterly. The few direct observations of surface current collected during FGGE (Katz and Garzoli, 1982) suggest that the zonal component of the ship drift currents are systematically high to the west by about 10 cm/s.

The distribution of surface current data is sparse, requiring interpolation to obtain monthly time-series at each 6° × 10° grid-point. The interpolation was performed subjectively by hand contouring the time versus longitude distributions of zonal current component for each 6° of latitude band shown in Figure 3. The contouring was performed giving most weight to quadrangles with greater than five points. Values of surface current were then picked off these distributions.

4. Oceanographic fields

Mean monthly distributions of SST during FGGE are given in MFM. Four representative distributions are given in Figure 4. As described in MFM, highest temperatures and smallest horizontal gradients are observed in late boreal winter and

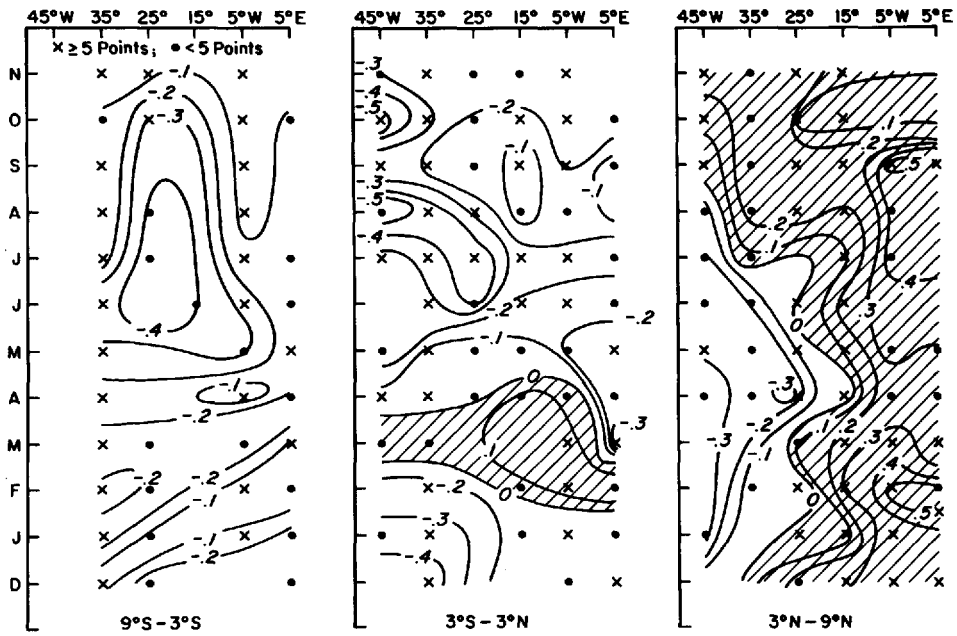

Figure 3. Observed and interpolated zonal components of surface velocity (m/s). The numbers represent the observations available during 1979.

early boreal spring, while lowest temperatures and largest gradients are observed in boreal summer and early boreal fall. Of particular importance to climate studies is the cold water tongue which appears on and south of the equator during boreal summer. In the region of the tongue, the 1979 SST's are somewhat higher (order of 1°C) than the climatological SST's given by Hastenrath and Lamb (1977), (Fig. 4).

In those regions where adequate data exist for a comparison, the 1979 mixed layer depth distributions are similar to the climatological distributions given by Lamb (1984) (Fig. 2). The shallowest mixed layers are observed in the eastern Atlantic throughout the year, with a deepening to the west (Fig. 5). The largest annual range in mixed layer depths is observed in the western Atlantic. Here, mixed layer depths vary by almost a factor of two, while in the eastern Atlantic, the range is less. In fact, for purposes of the heat balance computations, mixed layer depths are kept constant at the easternmost grid points.

In spite of the sparseness of surface current data and the inherent problems present in ship drift representations of this variable, the time series of zonal current component (Fig. 3) reproduce most of the major features reported on using direct current observations obtained during 1979 or given in climatological representations of the surface current field (Richardson and McKee, 1984). For instance, the North Equatorial Countercurrent (NECC) is observed to reverse direction seasonally in the

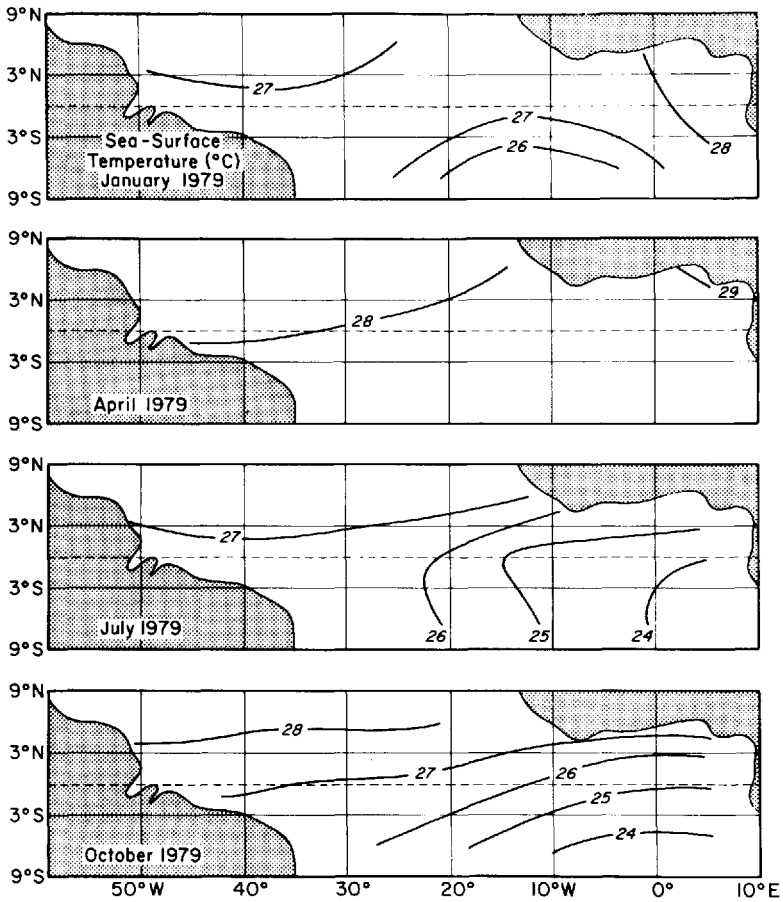

Figure 4. Representative sea-surface temperature (°C) distributions contoured on the 6° latitude by 10° of longitude grid.

western Atlantic but not in the eastern Altantic (Fig. 3). Garzoli and Richardson (1983) report a similar finding based on dynamic height differences across the latitude range of the NECC. Flow on the equator is to the east during late boreal winter and early spring and to the west at other times. Highest westward speeds are observed during early boreal summer with a secondary minimum in westward speeds observed during late summer. This latter minimum is probably related to the southward migration of the eastward flowing NECC during the summer. These features of equatorial flow reproduce the findings of Katz and Garzoli (1982); findings which were derived from direct observations of current obtained during 1979. Finally, the annual cycle of the zonal component of the South Equatorial Current (SEC) found in the ship-drift data between 9S and 3S (the band of maximum interpolation, Fig. 3) is characterized by minimum westward flow during boreal winter and maximum flow

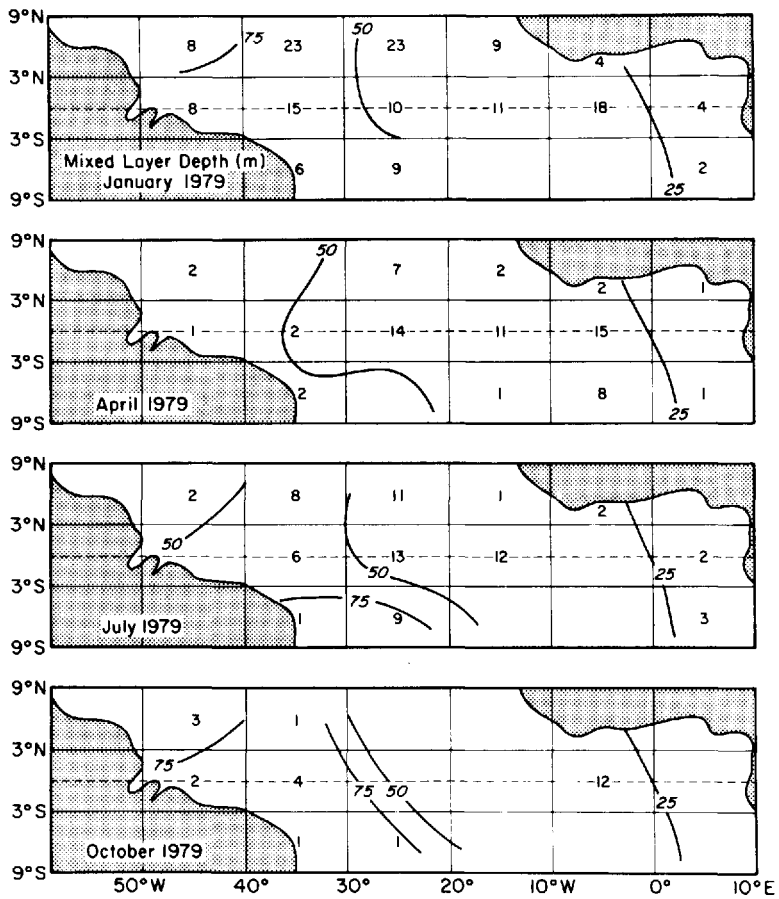

Figure 5. Same as Figure 4, except for mixed layer depth (m). Numbers represent available observations. The climatology of Lamb (1984) was used for interpolation in regions of little or no data.

beginning in late spring and continuing through the fall. Molinari (1983) observes a somewhat similar cycle in SEC intensity in a drifting buoy data set between 11S and 7S. However, in that data set low speeds exist through June.

Four distributions of net oceanic heat gain from MFM are given in Figure 6 for completeness. As noted in MFM, the large-scale patterns of heat gain during 1979 are very similar to those of Hastenrath and Lamb (1978). A systematic difference occurs in the boreal summer in the region of the cold water tongue. Here the 1979 oceanic heat gains are consistently less than those estimated from the climatological data set.

5. Application of the heat balance relationship

The balance between changes in mixed layer temperature and the surface heat flux represents a simplification of (1) which can be tested with the available data.

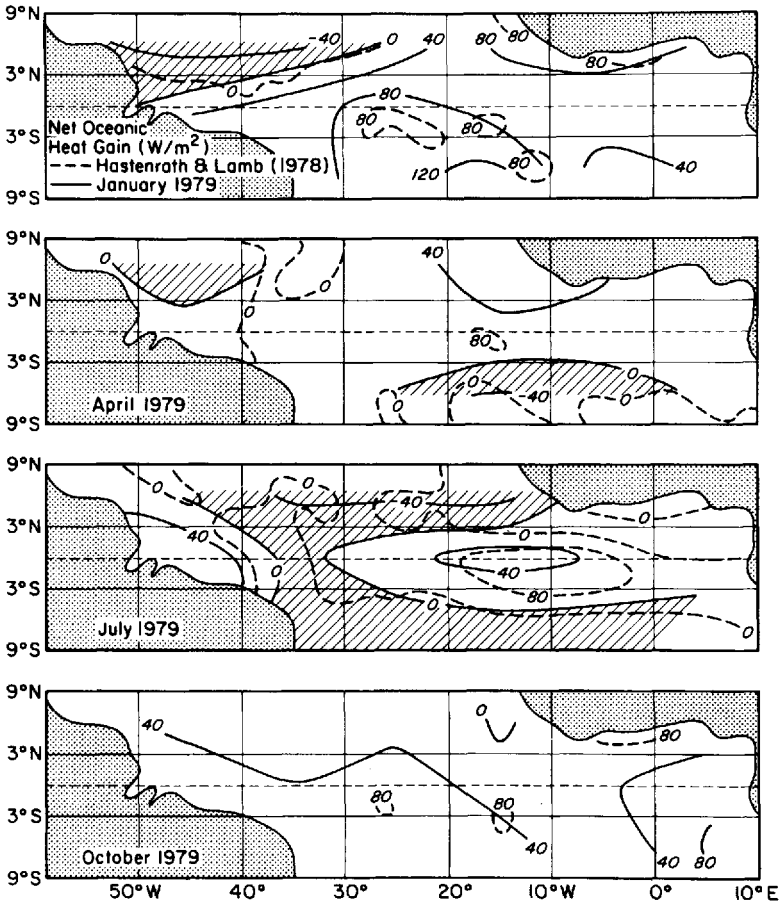

Figure 6. Same as Figure 4, except for net oceanic heat gain (W/m^2).

Neglecting all other terms but these, the integration of (1) yields

$$T_E(t) = \frac{1}{\rho c_p}\int_{t_1}^{t}\left(\frac{Q_o}{h}\right)' dt + \frac{1}{\delta t}\left[T(t_1) - T(t_0)\right](t - t_2) + T(t_2), \qquad (2)$$

where T_E represents an estimated mixed layer temperature determined only by surface fluxes. The arbitrary constant of integration $T(t_2)$ is chosen such that the mean of the estimated temperature time series is equal to the mean of the observed time series. As McPhaden (1982) stresses, (2) "predicts fluctuations and not actual values of mixed layer temperature."

Variances computed from the monthly time series of mixed layer temperature for each 6° × 10° quadrangle are shown in Figure 7. In general, variances increase monotonically from the northwestern portion of the grid to the southeastern portion of the grid. Highest variances represent an annual signal of over 2°C in the extreme

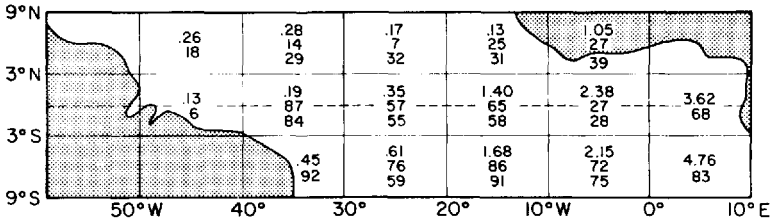

Figure 7. Within each 6° × 10° quadrangle, the top number represents the variance $(°C)^2$ in the observed monthly mixed layer temperature time series, the middle number represents the percentage variance in the observed time series accounted for by fluxes through the sea-surface and the lower number represents the percentage variance accounted for by fluxes through the sea-surface and zonal advection.

southeastern corner. Minimum variances represent an annual signal of about 0.5°C. The distribution of variances during 1979 (Fig. 7) is similar to the distribution of the amplitude of the annual harmonic given by Merle and LeFloch (1978).

Time series of the observed and estimated mixed layer temperatures are given in Figure 8. The coherence squared between the two time-series represents that portion of the variance in the observed series which can be accounted for by fluxes through the sea-surface (i.e., the variance reduction due to surface fluxes). The distribution of the coherence squared is also given in Figure 7. Largest variance reductions (>75%) are realized in the 9–3S band. Smallest reductions (<30%) occur in the 3–9N band and in the quadrangle centered at 0°, 5W.

Adding the effects of zonal advection to (2) results in the following relation,

$$T'_E(t) = \frac{1}{\rho c_p}\int_{t_2}^{t}\frac{Q'_o}{h}\,dt - \int_{t_2}^{t}\left(u\frac{\partial T}{\partial x}\right)'dt + \frac{1}{\delta t}[T(t_1) - T(t_0)]\,(t - t_2) + T(t_2). \quad (3)$$

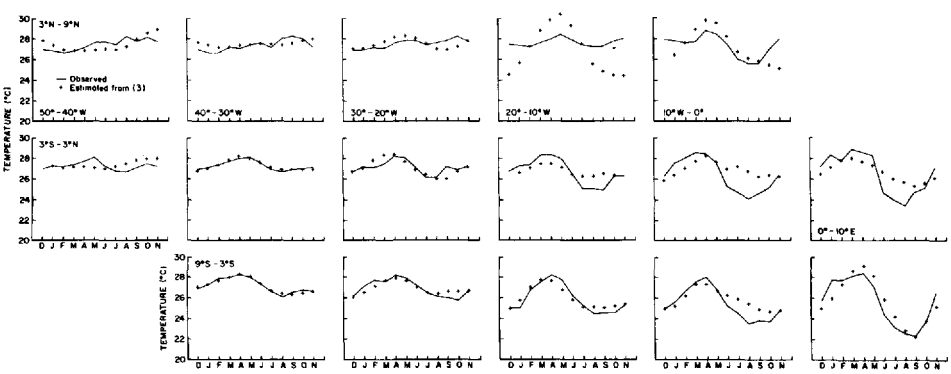

Figure 8. Time series of observed mixed layer temperatures (°C) and mixed layer temperatures estimated from Eq. (2).

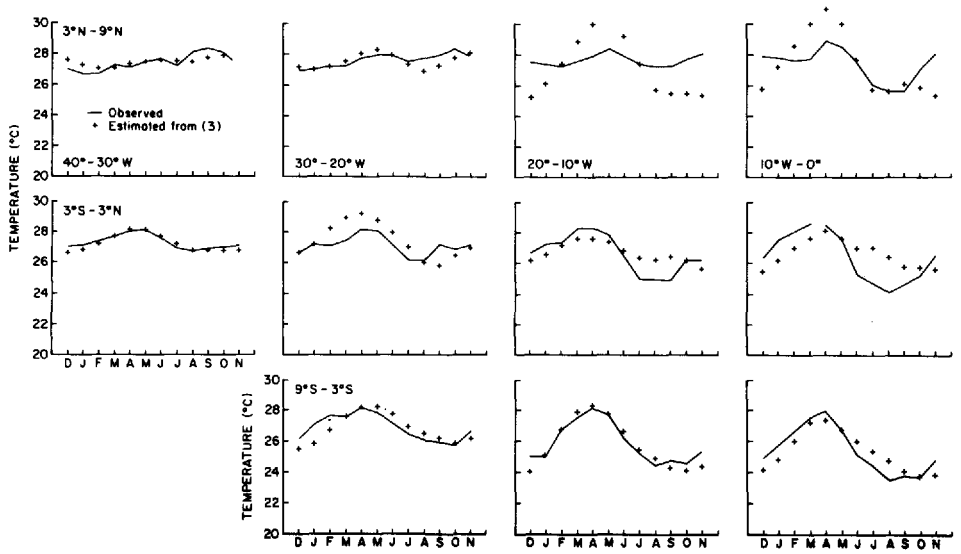

Figure 9. Time series of observed mixed layer temperatures and mixed layer temperatures estimated from Eq. (3).

Time series of observed temperatures and temperatures estimated from (3) are shown in Figure 9. The $\partial T/\partial x$ term cannot be evaluated by centered differences for the quadrangles along the eastern and western boundaries of the grid, so temperature estimates are not made for these points. The addition of zonal advection causes the largest improvement in variance reduction in the 3–9N band (Fig. 7). However, the improvements are not systematic; i.e., they do not improve the estimates in any particular season, and the variance reductions still remain less than 50%. There is some suggestion of systematic improvements in estimates along 6S during boreal summer. But here and along the equator changes in variance reductions are small.

The uncertainty in estimating the observed monthly change in mixed layer temperature ranges from about 0.3°C in the shipping lanes to about 0.6°C elsewhere, MFM. Largest errors in the rhs terms of (3) are related to uncertainties in estimates of net oceanic heat gain. MFM compute an uncertainty for Q_o estimates of 45 W/m^2 which translates, using a propagation of error analysis (Meyer, 1975), to errors in estimates of monthly temperature change ranging from 0.4°C (for a mixed layer depth of 75 m) to 1.0°C (for a mixed layer depth of 25 m). A 10 m uncertainty in mixed layer depth is equivalent to a 0.5°C uncertainty in temperature change, for a 25 m mixed layer depth and Q_o of 50 W/m^2. A similar error is associated with a 0.5°C/20° of longitude uncertainty in estimates of $\partial T/\partial x$. Uncertainties associated with 0.2 m/s errors in surface currents are also of the same order of magnitude. Thus, total uncertainty in estimating temperature changes from (3) is somewhat greater than 1.5°C.

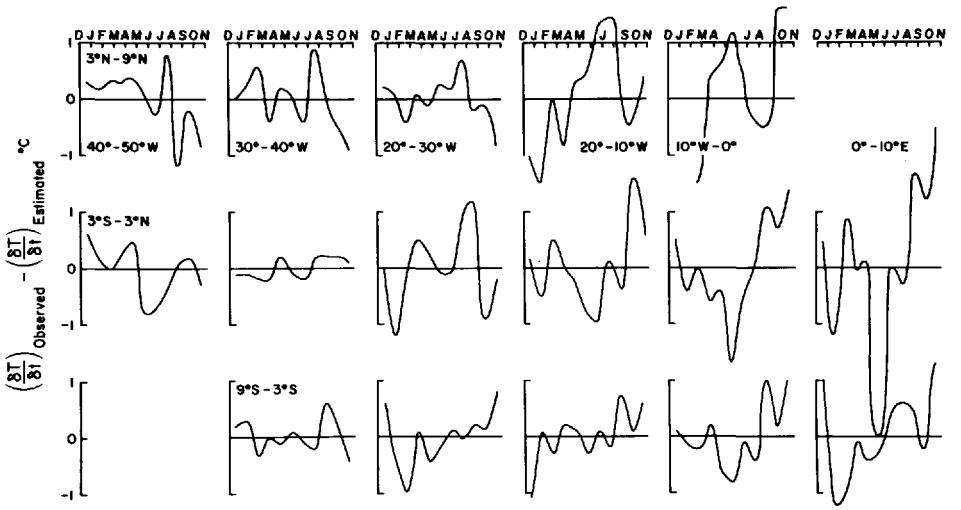

Figure 10. Time series of the differences between the observed monthly changes in mixed layer temperature and the temperature changes estimated from Eq. (3).

However, the large variance reductions along 6S (Fig. 7) indicate that actual errors, particularly in surface fluxes, are less. The rms difference between observed and estimated monthly temperature changes, (3), is about 0.5°C along 6S. A 0.5°C uncertainty in temperature change over one month is equivalent to an uncertainty in surface heat flux, from (2), of 20 W/m^2 for a 25 m thick mixed layer and 60 W/m^2 for a 75 m thick mixed layer. Since the differences between observed and estimated temperature changes also depend on errors in observed temperatures, average uncertainties in Q_o over the entire basin are probably closer to 20 to 30 W/m^2 than 45 W/m^2.

Plots of differences between observed and estimated temperature changes are given in Figure 10. If we assume that only differences greater than 0.5°C are significant, the only systematic differences which can be readily identified with specific physical processes are observed east of 20W along 0 and 6N. The estimates at 6N, 5W and 6N, 15W are too warm during boreal winter and summer, times of coastal upwelling in the Gulf of Guinea (Merle *et al.*, 1980). At 0, 15W, 0, 5W, and 0, 5E estimated temperatures are too high during boreal summer, the time of equatorial upwelling (Merle *et al.*, 1980). A possible qualitative explanation for this last feature is given next.

Vertical turbulent diffusion through the base of the mixed layer can be parameterized in several ways. Denman (1973), for instance, parameterizes this turbulence in terms of an entrainment velocity. Other investigators, who consider heat budgets of layers deeper than the mixed layer, use an eddy diffusivity to parameterize mixing (Wyrtki, 1981, for instance). Finally, McPhaden (1982) and Schopf and Cane (1983)

consider entrainment as the primary cause of vertical diffusion, but also include an eddy diffusivity term to represent a type of background dissipation which can act even in the absence of active entrainment. We choose to parameterize vertical diffusion in terms of entrainment as some data exist to evaluate this term at 0, 5W.

Denman (1973) and Niiler (1975), for instance, express vertical turbulent diffusion through the base of the mixed layer as

$$Q_{-h} = \omega_e \Delta T = \left(\frac{dh}{dt} + \omega\right)\Delta T, \tag{4}$$

where ω_e, the entrainment velocity, is defined in terms of the changes in mixed layer depth, dh/dt, and the vertical velocity of particles below the base of the mixed layer, ω. Entrainment is defined only for periods of positive ω_e and is assumed zero for periods of negative ω_e. ΔT represents the change in temperature across the base of the mixed layer. Changes in mixed layer depth are small at 0, 5W throughout the year and have been assumed to be zero. Voituriez (1981) shows a time history of the depth of the 160 cl/t isanosteric surface obtained during FGGE at 0, 4W. Although this surface is deeper than the base of the mixed layer, at approximately 100 m, for purposes of this simple calculation, changes in the depth of the 160 cl/t surface are used to evaluate ω.

Positive ω's indicative of upwelling occur from about 1 April through 1 August. Values of ω ranged from about 3×10^{-7} m/s during April and July to about 7×10^{-7} m/s during May and June. Negative ω's and therefore no possible entrainment occur during the other months. If ΔT is taken as 1°C, Q_{-h} ranges from 10 W/m^2 during April and July to 30 W/m^2 during May and June. Rewriting (3) to include Q_{-h}, a new time series of estimated SST which now includes the effects of surface fluxes, zonal advection and turbulent diffusion can be computed. Coherence squared between the estimated and observed SST series is 0.6. The series with diffusion accounts for more variance than the series without diffusion (Fig. 7) because of a more realistic representation of the cooling at 0, 5W during boreal summer. The absence of suitable data in the quadrangles within which coastal upwelling is observed precludes similar computations. However, it is not unreasonable to assume that similar improvements in variance reduction can be realized in these regions by including vertical diffusion.

The effects of meridional advection are not quantified because of the lack of adequate data to resolve the meridional current field. A qualitative estimate of these effects is offered. In the eastern Atlantic, largest meridional temperature gradients are observed during boreal summer, fall and early winter. Gradients are of the order of 2°C/(6° of latitude). If these gradients are coincident with a northward flow of 0.1 m/s, associated changes in heat content are of the order of 30 W/m^2. Thus, meridional advections can have an impact on SST of the same order as vertical diffusion.

6. Summary and discussion

The lack of significant variance reduction along 6N, west of 20W, is probably related to both the lower variances observed here (Fig. 7) and the uncertainties in estimates of the various terms in (3). The significant variance reductions along 6S suggest that a large portion of the asymmetry observed in the boreal summer cold water tongue can be attributed to surface fluxes alone. As mentioned previously, the systematic differences between observed and estimated temperature changes in the quadrangles centered at 6N, 15W, 6N, 5W and 0, 5W can be characterized by inadequate cooling during periods of either coastal or equatorial upwelling. Data are insufficient to estimate quantitatively the magnitude of those terms in (1) not evaluated above. However, some qualitative estimates of the effect of vertical turbulent diffusion and meridional advection in the quadrangle centered at 0, 5W suggest that both terms contribute to the heat budget of the mixed layer.

MFM note that although net oceanic heat gain during FGGE was anomalously low when compared to the climatology of Hastenrath and Lamb (1978), SST's were anomalously high. Data are not available to determine the "normalcy" during FGGE of the oceanic processes which contribute to surface cooling or heating. Thus, it is not possible to ascertain if the effects of anomalies in entrainment or meridional advection caused the higher SST's. Furthermore, although zonal advection did not play an important role in establishing SST during FGGE, we cannot say if this is the average condition or an anomaly. Numerical models, which include non-adiabatic processes in the upper layers, using the FGGE winds, are required to address these questions.

Merle (1980) computed heat content changes in equatorial Atlantic boxes 8° of latitude by 4° of longitude, extending from the sea-surface to 300 m. He finds largest variance in the west where the thermocline is deepest and smallest variance in the east where the thermocline is shallowest. He also finds a boreal summer minimum in the annual heat content series and suggests that this minimum propagates from west to east. In contrast, since we only consider mixed layer temperatures, largest variances are in the east (Fig. 7). Furthermore, we do not observe a west to east propagation of the boreal summer minimum in SST along the equator (Fig. 8). Thus some care must be taken when inferring changes in SST from changes in heat content computed over deeper water columns.

Acknowledgments. This work was partially funded by the NOAA Special Research Programs Office. We wish to thank the British Meterological Office for supplying the ship-drift data.

REFERENCES

Denman, K. L. 1973. A time-dependent model of the upper ocean. J. Phys. Oceanogr., *3*, 173–184.

Garzoli, S. L. and P. L. Richardson. 1983. Seasonal variations of the Atlantic North Equatorial Countercurrent. Tropical Ocean-Atmospheric Newsletter, No. 20, (unpublished manuscript).

Hastenrath, S. 1980. Heat budget of tropical ocean and atmosphere. J. Phys. Oceanogr., *10,* 159–170.

Hastenrath, S. and P. Lamb. 1977. Climatic Atlas of the Tropical Atlantic and Eastern Pacific Oceans. University of Wisconsin Press.

—— 1978. Heat Budget Atlas of the Tropical Atlantic and Eastern Pacific Oceans. University of Wisconsin Press.

Katz, E. J. and S. Garzoli. 1982. Response of the western equatorial Atlantic Ocean to an annual wind cycle. J. Mar. Res., *40* (Suppl.), 307–327.

Lamb, P. J. 1984. On the mixed layer climatology of the north and tropical Atlantic. Tellus, *36A,* 292–305.

McPhaden, M. J. 1982. Variability in the central equatorial Indian Ocean, Part II: Oceanic heat and turbulent energy balances. J. Mar. Res., *40,* 403–419.

Merle, J. 1980. Seasonal variation of heat-storage in the tropical Atlantic Ocean. Oceanologica Acta, *3,* 455–463.

Merle, J., M. Fieux and P. Hisard. 1980. Annual signal and interannual anomalies of sea surface temperature in the eastern equatorial Atlantic Ocean, *in* Equatorial and A-Scale Oceanography, W. Duing, ed., Supp. II to Deep-Sea Res., *26A,* 77–101.

Merle, J. and J. LeFloch 1978. Cycle annuel moyen de la temperature dans les couches superieures de l'Ocean Atlantique intertropical. Oceanologica Acta, *1,* 271–276.

Meyer, S. L. 1975. Data Analyses for Scientists and Engineers. John Wiley, New York, 513 pp.

Molinari, R. L. 1983. Observations of near-surface currents and temperature in the central and western tropical Atlantic Ocean. J. Geophys. Res., *88,* 4433–4438.

Molinari, R. L., J. F. Festa and E. Marmolejo. 1984. Evolution of sea-surface temperature and surface meteorological fields in the tropical Atlantic Ocean during FGGE, 1979: Part I, description of surface fields and computation of surface energy fluxes. Prog. in Oceanogr., (in press).

Molinari, R. L., E. Katz, E. Fahrbach, H. U. Lass and B. Voituriez. 1983. Near surface temperature observations obtained in the equatorial Atlantic Ocean during FGGE 1979, *in* Hydrodynamics of the Equatorial Ocean, J. C. J. Nihoul, ed., Elsevier Science Publishers, Amsterdam, 65–82.

Niiler, P. P. 1975. Deepening of the wind-mixed layer. J. Mar. Res., *33,* 405–422.

Niiler, P. P. and W. J. Stevenson. 1982. The heat budget of tropical ocean warm water pools. J. Mar. Res., *40* (Suppl.), 465–480.

Richardson, P. L. and T. K. McKee. 1984. Average seasonal variation of the Atlantic Equatorial Currents from historical ship drifts. J. Phys. Oceanogr., *14,* 1226–1238.

Schopf, P. S. and M. A. Cane. 1983. On equatorial dynamics, mixed layer physics and sea surface temperature. J. Phys. Oceanogr., *13,* 917–935.

Voituriez, B. 1981. The equatorial upwelling in the eastern Atlantic Ocean, *in* Recent Progress in Equatorial Oceanography: A Report of the Final Meeting of SCOR Working Group 47 in Venice Italy, J. P. McCreary, D. W. Moore, and J. M. Witte, eds., Nova Univ./NYIT Press, Fort Lauderdale, FL, 229–248.

Wyrtki, K. 1981. An estimate of equatorial upwelling in the Pacific. J. Phys. Oceanogr., *11,* 1205–1214.

Received: *19 June, 1984;* revised: *5 October, 1984.*